Icarus 226 (2013) 510–521

Contents lists available at SciVerse ScienceDirect

Icarus

journal homepage: www.elsevier.com/locate/icarus

Predicted crater morphologies on Ceres: Probing internal structure and evolution

Michael T. Bland *

Department of Earth and Planetary Sciences, Washington University in St. Louis, Saint Louis, MO 63130, United States
McDonnell Center for the Space Sciences, Washington University in St. Louis, Saint Louis, MO 63130, United States

ARTICLE INFO

Article history:
Received 7 March 2013
Revised 22 May 2013
Accepted 25 May 2013
Available online 7 June 2013

Keywords:
Asteroid Ceres
Cratering
Ices
Tectonics
Interiors

ABSTRACT

The detailed internal structure of the dwarf planet Ceres, target of NASA's *Dawn* mission, has not been unequivocally determined from ground-based data. Whereas Ceres is most likely differentiated with a near surface ice layer tens to one-hundred kilometers thick, the possibility of a homogenous, ice-poor interior structure cannot be completely eliminated. These two internal structural end-members have profoundly different implications for Ceres' origin and evolution. Here we demonstrate that observations of Ceres' impact craters by the *Dawn* spacecraft will permit unambiguous distinction between the two internal structural models. Using finite element simulations of crater relaxation, we show that if Ceres *does* contain a water ice layer, its relatively warm diurnally-averaged surface temperature ensures extensive viscous relaxation of even small impact craters. At likely equatorial temperatures, craters as small as 4-km in diameter can be relaxed to the point where complete crater erasure is plausible, thus decreasing the overall crater density in the equatorial region. At mid-latitudes, crater relaxation is less extensive, but still sufficient to completely relax all craters older than 10 Ma and larger than ~16 km in diameter, as well as smaller, ancient craters. Only in Ceres' cold polar regions are some crater morphologies expected to be pristine. In contrast, if Ceres is primarily a rocky body, we expect crater relaxation to be negligible. These basic conclusions are generally independent of ice grain size, salt/dust contamination of the ice, the presence of a thin, undifferentiated ice/rock crust, and the total thickness of the ice layer, all of which produce second-order modifications to the relaxation process that can be used to better constrain such ice layer properties. Thus, the morphology of impact craters on Ceres, as revealed by the *Dawn* spacecraft, will provide direct insight into the internal structure and evolution of the dwarf planet.

1. Introduction

The dwarf planet Ceres constitutes roughly one-third of the mass of the asteroid belt. Broadly classified as a carbonaceous asteroid (compositionally), ground-based spectroscopy indicates that its surface includes hydrated minerals (e.g., brucite, $Mg[OH]_2$, Milliken and Rivkin, 2009), carbonates (e.g., dolomite, Rivkin et al., 2006; Milliken and Rivkin, 2009), iron-rich clays (cronstedtite, Rivkin et al., 2006; Milliken and Rivkin, 2009), and possibly magnetite (Rivkin et al., 2011). While these minerals are consistent with hydrous alteration (e.g., Lebofsky, 1978; Rivkin et al., 2011), water ice itself, which is thermodynamically unstable on Ceres' surface (e.g. Fanale and Salvail, 1989), has not been observed (though see Lebofsky et al., 1981; Vernazza et al., 2005). Detection of water vapor near Ceres' limb (possibly the result of sublimation of a polar frost layer) by A'Hearn and Feldman (1992) has not be confirmed by subsequent investigations (Rousselot et al., 2011).

Despite the absence of free water on its surface, Ceres' low density (2077 kg m^{-3} (Thomas et al., 2005); 2206 kg m^{-3} (Carry et al., 2008)) suggests it may contain large amounts of water ice internally. McCord and Sotin (2005) argued from thermal evolution models that short-lived and/or long-lived radiogenic heating is sufficient to completely melt any water ice on the body, resulting in complete differentiation of Ceres (excepting a thin surface "crust", see below). The theoretical prediction of a differentiated Ceres was subsequently confirmed by Thomas et al. (2005) and Carry et al. (2008), who argued from Hubble Space Telescope (HST) observations and Keck near-IR data that the shape of Ceres (i.e., its $J2$) is consistent with a differentiated body (see also McCord et al., 2006). The shape and density measurements are consistent with a body that contains an ice layer 30–80 km thick sandwiched between a relatively thin, rocky, surface lag and a large rocky core (McCord and Sotin, 2005; Thomas et al., 2005; Carry et al., 2008). These initial models were confirmed and refined by Castillo-Rogez and McCord (2010) who showed that the rocky core may be further differentiated into hydrated and dehydrated layers.

* Address: Department of Earth and Planetary Sciences, Washington University in St. Louis, Saint Louis, MO 63130, United States. Fax: +1 314 935 7361.
E-mail address: mbland@levee.wustl.edu

0019-1035/$ - see front matter © 2013 Elsevier Inc. All rights reserved.
http://dx.doi.org/10.1016/j.icarus.2013.05.037

Alternatively, Zolotov (2009) argued that the near-IR shape measurements of Carry et al. (2008) are also consistent with an undifferentiated body, and posited a Ceres with high average porosity, and composed of low-density material. Whereas it is arguable whether such an internal structure is plausible from a thermal-evolution perspective (e.g., Castillo-Rogez, 2011), current data cannot unambiguously distinguish between the two different internal structural models.

The two different internal structures have profoundly different implications for Ceres' geophysical evolution and astrobiological potential. A differentiated structure suggests early accretion, after which substantial hydrothermal activity could be driven by the decay of short-lived radiogenic species ^{26}Al and ^{60}Fe (Castillo-Rogez and McCord, 2010). The hydrothermally altered core could later dehydrate, with the associated volume changes causing disruption of Ceres' surface (i.e., geologic activity) (McCord and Sotin, 2005). Such dehydration would create a layered core structure that could enable partial melting of the silicates (Castillo-Rogez and McCord, 2010). Differentiation also occurs readily if Ceres accreted later, after the decay of short-lived radiogenic species, though core hydrothermal activity (as well as dehydration) are unlikely in such a scenario (McCord and Sotin, 2005; Castillo-Rogez and McCord, 2010). Significantly, some thermal evolution models permit the present-day existence of a deep liquid water layer on Ceres (McCord and Sotin, 2005; Castillo-Rogez and McCord, 2010). The presence of liquid water, chemical gradients, and plausibly organics would suggest significant astrobiological potential (Castillo-Rogez and Conrad, 2010). Furthermore, abundant free water on Ceres might suggest that it originated deeper in the Solar System (i.e., the Kuiper belt) and was later dynamically scattered to its current location (semi-major axis a of 2.77 AU) (McKinnon, 2008, 2012).

In contrast, if Ceres is an undifferentiated rocky body it must consist of low-density hydrated material (grain density similar to CI chondrites) such as phyllosilicates, hydrated salts, and plausibly organics (Zolotov, 2009). This implies that Ceres accreted late (to avoid dehydration by intense short-lived radiogenic heating) from pervasively hydrated planetesimals, and subsequently avoided porosity collapse during heating by long-lived radiogenic species (Castillo-Rogez, 2011). The surface of such a body would likely display little evidence of an active geologic past, and without liquid water, Ceres would have little astrobiological potential.

Castillo-Rogez and McCord (2010) and McCord et al. (2011) pointed out that, if Ceres does contain a relatively thick ice layer, surface topography should quickly viscously relax at Ceres' warm surface temperatures. Assuming an isothermal temperature structure and a surface temperature of 180 K (see below), simple calculation of the e-folding timescale (τ) for viscous relaxation of topographic wavelengths (λ) as short as 100 m is only ~1 Ga (i.e., $\tau = (4\pi\eta)/(\rho g\lambda)$, where ρ is the density, g is the gravitational acceleration, and $\eta = \eta_o \exp[l(T_m/T - 1)]$ is the viscosity, where $\eta_o = 10^{14}$ Pa s is the melting point viscosity, T_m and T are the melting temperature and temperature, respectively, and $l = 26$ is the non-dimensional constant Q/RT_m, where $Q = 60$ kJ mol^{-1} is the activation energy, and R is the gas constant).

Such simple calculations suggest that Ceres could be extremely smooth (as was once proposed for icy satellites (Johnson and McGetchin, 1973)), and ground based imaging supports that notion. Spatially resolved images of Ceres suggest that its surface is extremely bland, with UV, visible, and IR albedo variations of only ~6% at the limits of resolution (typically ~60 km/pixel) (Li et al., 2006; Carry et al., 2008). Ceres also appears to be compositionally homogeneous, with little variation in spectral signature across the surface (Rivkin and Volquardsen, 2010; Carry et al., 2012). Although a uniform surface does not necessarily imply a topographically smooth surface, HST measurements of Ceres' shape indicate that the body does not deviate from a relaxed spheroid by more than 5 km (Thomas et al., 2005). Carry et al. (2008) report maximum ellipsoidal fit residuals of 18 km (notably, Ceres' HST- and Keck-derived equatorial dimensions differ by ~10 km). Current resolution is insufficient, however, to detect limb topography (e.g., craters) with wavelengths smaller than ~60 km in diameter, and topographic relief of 8 km or more could escape detection (Thomas et al., 2005). Thus, further constraining Ceres' interior from ground-based shape/topography data will prove challenging.

Fortunately, NASA's *Dawn* spacecraft will soon enter orbit around Ceres (arrival in early 2015), with level-1 science goals of imaging 80% of the surface at a resolution of 200 m/pixel or better, and obtaining a topographic map of 80% of the surface with 200 m horizontal, and 20 m vertical, resolution (Russell and Raymond, 2011). Achievement of these goals will permit detailed topographic and morphological characterization of Ceres' surface, including its impact craters. Such characterization will allow a determination of both the simple-to-complex crater transition diameter and the relaxation state of Ceres' impact craters. Here we describe how each of these analyses can be used to infer whether Ceres contains an internal ice layer. First we discuss Ceres' simple-to-complex transition diameter and what it implies for Ceres' near surface composition. We then describe numerical simulations of crater relaxation under Ceres-like conditions that account for the complex rheology of water ice, the decrease in radiogenic heat flux over Solar System history, and the latitudinal variation in Ceres' surface temperature. These simulations indicate that relaxation of impact craters is inevitable over much of Ceres' surface *if* an ice layer is present. In contrast, no relaxation is expected if Ceres is an undifferentiated rocky body. Thus, observations of Ceres' craters by the *Dawn* spacecraft will permit unambiguous distinction between the two internal structural models described above.

2. Simple–complex transition diameter

The diameter at which impact craters transition from "simple" bowl-shaped craters to "complex" craters with terraced walls and central structures (e.g., uplifts, rings, pits) is a function of both the surface gravity and the target material (Pike, 1980; Schenk, 1991; Schenk et al., 2004). Fig. 1 shows the simple-to-complex transition diameter (hereafter referred to simply as the transition diameter)

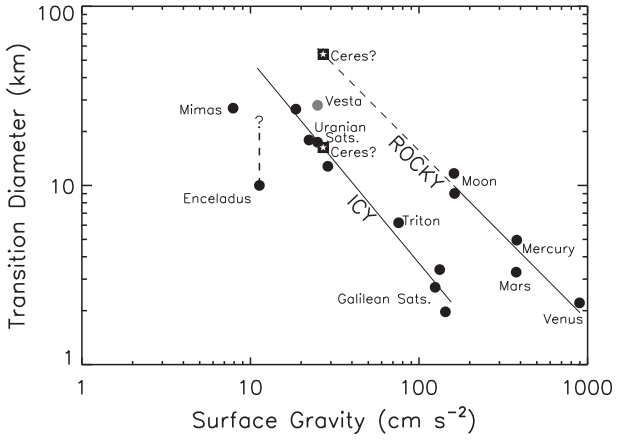

Fig. 1. Simple-to-complex transition diameter as a function of surface gravity for icy and rocky bodies across the Solar System (after Schenk et al., 2004). The hypothetical transition diameters for an "icy" and "rocky" Ceres are indicated with a white star on a black square. The plot includes preliminary estimates of the transition diameter of Vesta (gray circle, see text). The transition diameter for Enceladus (uncertainty indicated by the vertical dashed line) is poorly constrained because of extensive crater modification (see Bland et al., 2012).

on bodies across the Solar System. In general, the transition occurs at smaller crater diameters for higher surface gravities and rocky (as opposed to icy) bodies. The clear distinction between the transition diameters on icy and rocky bodies may therefore be diagnostic of Ceres' near surface composition. If Ceres' near surface is predominantly icy, then its surface gravity of 27 cm s^{-2} suggests a transition diameter near 16 km. If, on the other hand, Ceres is primarily a rocky body (as suggested by Zolotov (2009)) then Ceres' transition diameter could potentially be much higher, near 50 km.

Few studies of crater morphometry have been performed on rocky bodies with surface gravity as low as Ceres. Preliminary work determining the transition diameter of craters on rocky Vesta (which has a similar surface gravity to Ceres) suggests that the transition occurs near 28 km (Schenk et al., 2013), which is much lower than expected for a silicate body based on extrapolation from larger rocky bodies. Large craters on Vesta have a transitional morphology with characteristics of both "simple" and "complex" craters, complicating the definition of transition diameter (Schenk et al., 2013). Furthermore, Ceres' surface rock is hydrated "soft rock," akin to martian or terrestrial sedimentary terrains. The transition diameter on an undifferentiated Ceres might therefore by lower than expected if extrapolated from "hard rock" bodies like the Moon and Mercury (Pike, 1980). Yet, Vesta's relatively low transition diameter of 28 km is substantially higher than that expected for an icy body with Ceres' surface gravity. Thus, we suggest that a transition diameter of 10–20 km on Ceres would indicate the presence of a relatively thick icy layer, whereas a transition diameter greater than 20 km would suggest a purely rocky interior. Determination of the transition diameter on Ceres may, however, be complicated by the influence of its rocky surface lag, and by the effects of viscous relaxation, which (as discussed below) is expected to alter crater morphologies across most of Ceres' surface. Thus, any determination of Ceres' transition diameter should not be over-interpreted.

3. Modeling viscous relaxation on Ceres

Whereas the transition diameter provides some insight into Ceres' near surface composition, a more robust inference can be made from the examination of the relaxation state of Ceres' impact craters. We use the finite element model Tekton2.3 (Melosh and Raefsky, 1980) to simulate crater relaxation on Ceres following the basic modeling approach described in Bland et al. (2012). We focus our investigation on the viscous relaxation of small craters with diameters (D) from 4 to 20 km. Based on the transition diameters described above, we assume all craters to be "simple," with parabolic shapes, depth to diameter ratios of $d = 0.2D$, rim heights of $h_{rim} = 0.036D$, and ejecta thicknesses that decreases as $r^{1/3}$ (Melosh, 1989). These craters are small enough to avoid the complicating effects of Ceres' radius of curvature (a 20 km diameter crater transverses just ~2.5° on Ceres). Because viscous relaxation timescales increase with decreasing topographic wavelength (see analytical formula above), small craters provide the greatest constraints on the pervasiveness of topographic relaxation. That is, if a crater with a diameter of 20 km fully relaxes under a given set of conditions, then it can reasonably be assumed that all larger craters will also be fully relaxed. The exception may be very large craters (e.g., $D > 100$ km), for which Ceres' radius of curvature and rocky core may influence relaxation (see Section 4.3.3). A select number of simulations were performed with larger craters (e.g., $D = 52$ km) to better constrain relaxation rates in Ceres' colder polar regions. We assume craters with $D > 20$ km are complex (see Section 2), and their shapes were informed by craters on mid-sized Saturnian satellites (White and Schenk, 2011).

Our standard axisymmetric simulation domain is five crater radii in depth and radius, ensuring the bottom and side boundaries have negligible influence on the results (see further discussion in Section 4.3.3). The sides of the domain are free slip in the vertical (z) direction and fixed in the radial (r), while the bottom boundary is fixed in both r and z. The top of the domain is a free surface upon which the crater topography is imposed. Each mesh has a horizontal resolution of one-tenth of the crater radii (e.g., 200 m for a crater with $D = 4$ km, 1 km for a crater with $D = 20$ km). The vertical resolution varies from 100 m for the smallest craters to 400 m for the largest. These resolutions are more than sufficient to resolve the low heat fluxes expected on Ceres (see below) while maintaining numerical efficiency.

We impose an initial stress state that approximates a static fluid initial stress state (i.e., "Poisson stresses" are neglected) assuming a density (ρ) of 930 kg m^{-3} (cold and dense). The crater topography perturbs this stress field such that the total initial stress field is given by (Dombard and McKinnon, 2006),

$$\sigma_{rr} = \sigma_{zz} = \sigma_{\theta\theta} = -\rho g\left\{z - h(r)\exp\left[\frac{h(r)-z}{D/2\pi}\right]\right\} \quad (1)$$

where z is the depth (0 at the surface), g is the acceleration of gravity at Ceres' surface (0.27 m s^{-1}), D is the crater diameter, and $h(r)$ is the height of the topography. The stress perturbation decays exponentially with depth with a wavelength of $D/2\pi$.

In our nominal simulations we assume a pure viscoelastic ice rheology including all relevant creep mechanisms for ice: three dislocation creep regimes, grain boundary sliding (GBS), basal slip (BS), and diffusion creep. The GBS and BS mechanisms are rate limiting such that the composite flow law has the form (Durham and Stern, 2001; Durham et al., 2010)

$$\dot{\varepsilon}_{visco} = \dot{\varepsilon}_A + \dot{\varepsilon}_B + \dot{\varepsilon}_C + [(1/\dot{\varepsilon}_{GBS}) + (1/\dot{\varepsilon}_{BS})]^{-1} + \dot{\varepsilon}_{diff} \quad (2)$$

where each $\dot{\varepsilon}$ refers to the strain rate for each rheological mechanism as denoted by the subscripts A, B, C, GBS, BS, and $diff$, and $\dot{\varepsilon}_{visco}$ is the total viscous strain rate. The constitutive relationship for each viscous flow mechanism has the general form

$$\dot{\varepsilon} = A(1/d)^m \acute{\sigma}^n \exp(-Q/RT) \quad (3)$$

where n is the power law exponent, A is a rheological constant, d is the grain size, m is the grain size exponent, $\acute{\sigma}$ is the deviatoric stress, Q is the activation energy, R is the gas constant, and T is the temperature. The rheological parameters used in our simulations are from the compilation in Durham and Stern (2001) and are provided in Table 1. Diffusion creep is modeled following the approach of Barr and Pappalardo (2005) who cast volume diffusion in the form of Eq. (3) by defining an effective A based on the diffusion parameters of Goldsby and Kohlstedt (2001). We use a Young's modulus of 9.33 GPa, and a Poisson's ratio of 0.325 (Gammon et al., 1983). We implicitly assume that Ceres' surface lag of rocky material does not affect the mechanical properties of the intact ice at depth. Both the GBS mechanism and diffusion creep are grain-size sensitive. The ice grain size in the interiors of icy bodies throughout the Solar System is unknown (see discussion in Bland and McKinnon, 2012a). We assume an ice grain size of 1 mm, consistent with terrestrial polar glaciers (e.g., Souchez and Lorrain, 1991), theoretical models of grain size evolution during convection of icy bodies (Barr and McKinnon, 2007), and our previous work (Bland et al., 2012). The effect of ice grain size on crater relaxation is discussed in Section 4.2. Typical differential stresses ($\sigma_{rr} - \sigma_{zz}$) are less than 0.1 MPa, with maximum stresses of 0.25 MPa. Under these conditions GBS dominates the rheology beneath the crater, with diffusion creep (which is enabled by the low stresses and warm temperatures) making a substantial contribution deeper in the mesh (cf. Fig. 1 in Barr and Pappalardo (2005)). For a subset of simulations we also examine the rheological effects of "dirty" ice (see Section 4.3.1 for further discussion).

Table 1
Rheological parameters.

Creep regime	$\log A$ ($MPa^{-n} m^m s^{-1}$)	m	n	Q (kJ $mole^{-1}$)	Reference
Dislocation creep					
Regime A	11.8	0	4.0	91	Kirby et al. (1987)
Regime B	5.1	0	4.0	61	Kirby et al. (1987)
Regime C	−3.8	0	6.0	39	Durham et al. (1997)
GBS	−2.4	1.4	1.8	49	Goldsby and Kohlstedt (2001)
BS	7.74	0	2.4	60	Goldsby and Kohlstedt (2001)
Volume diffusion	−3.46	2	1.0	59.4	Goldsby and Kohlstedt (2001) and Barr and Pappalardo (2005)

3.1. Viscosity structure and radiogenic heat flux

The viscosity structure of the lithosphere is set by the vertical temperature profile through the domain, which is set by the prescribed heat flux and the surface temperature. Tekton does not explicitly include thermodynamics; however, we can prescribe a time-dependent heat flux consistent with the decay of long-lived radiogenic species on Ceres and update the viscosity structure accordingly. The abundance of radiogenic species depends on Ceres' rock fraction, which depends on its assumed internal structure. The thickness of Ceres' rock and ice layers as a function of silicate density are shown in Fig. 2 assuming a simple mass balance (density of 2206 kg m^{-3} (Carry et al., 2008), and average radius of 470 km), and a differentiated internal structure. For our relaxation calculations, we assume a silicate density of 2700 kg m^{-3}, which implies a rock core 421 km in radius with a mass of 8.44×10^{20} kg. We assume a CI chondrite-like complement of radiogenic species (abundances from Lodders and Fegley, 1998). The resulting steady-state heat flux as a function of time is shown in Fig. 2. With these assumptions the maximum heat flux on Ceres at Solar System formation was ~7.5 mW m^{-2} (neglecting short-lived radiogenic species and transient effects from accretion), whereas at 4 Ga (during or just before the Late Heavy Bombardment) the heat flux was 5.6 mW m^{-2}. The current heat flux is just less then 1 mW m^{-2}. Increasing or decreasing the assumed rock fraction has only a small effect on the calculated heat flux, especially within the last 100 Ma.

The thermal conductivity (k) of ice is temperature dependent with the form $k = 651\ \mathrm{W\ m^{-1}}/T$, where T is the temperature (Petrenko and Whitworth, 1999). For a heat flux q at time t, the temperature as a function of depth z is give by

$$T(z) = T_s \exp(qz/651\ \mathrm{W\ m^{-1}}) \quad (4)$$

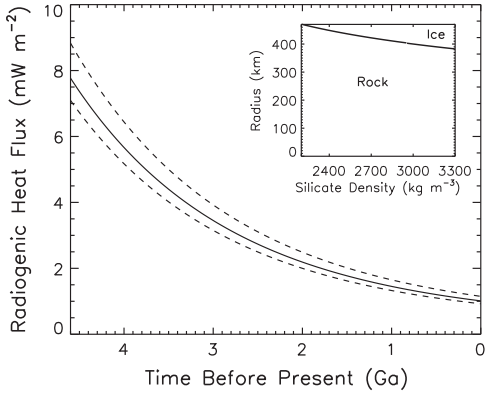

Fig. 2. The steady-state heat flux as a function of time due to long-lived radiogenic species, assuming a CI chondrite composition. The solid line is the flux used in the simulations discussed here (assuming a silicate density of 2700 kg m^{-3}). Dashed lines correspond to maximum and minimum plausible heat fluxes (i.e., a pure rock Ceres with density of 2206 kg m^{-3}, and a Ceres with large ice layer and a rock density of 3300 kg m^{-3}). The inset shows the radius of the rocky core resulting from simple mass balance calculations of Ceres' internal structure as a function of assumed silicate density.

where T_s is the surface temperature (Fig. 3). We limit the maximum temperature in the domain to 250 K, at which point the mesh becomes isothermal. In a few cases a maximum temperature of 200 K was used for numerical efficiency; however, using the cooler limit had a negligible effect on crater relaxation (see also Dombard and McKinnon, 2006).

The heat flux is updated every 10^4 timesteps. The timestep size is dynamic and based on the minimum Maxwell time in the simulation domain ($T_m = \eta/\mu$, where μ is the shear modulus and η is the effective viscosity). Simulations with warm surface temperatures and/or high heat fluxes (i.e., older craters) require the shortest timestep. Typical timestep values range from 10 to 10^4 years, resulting in the heat flux being updated every 10^5 to 10^8 years. Even when only updated every 100 Ma the heat flux changes by less than 5% between updates.

3.2. Surface temperature

For the low heat fluxes expected on Ceres, the surface temperature dominates the temperature structure. A present-day heat flux of 1 mW m^{-2} results in a nearly isothermal temperature structure with $T(z) \approx T_s$ (Fig. 3). The surface temperature is thus a primary control on viscous relaxation (see also Bland et al., 2012). The temperature of Ceres' surface has not been directly measured, so determining the variation in surface temperature with latitude requires a theoretical approach. We follow Ojakangas and Stevenson (1989), who calculated long-term diurnally averaged surface temperatures for Europa. We have recently shown that these temperatures provide a reasonable match to diurnally-averaged latitudinal temperature variations derived from Galileo Photopolarometer-Radiometer data (Bland and McKinnon, 2013). The long-term, diurnally-averaged surface temperature (T_s) as a function of co-latitude on Ceres (θ) is given by (Ojakangas and Stevenson, 1989)

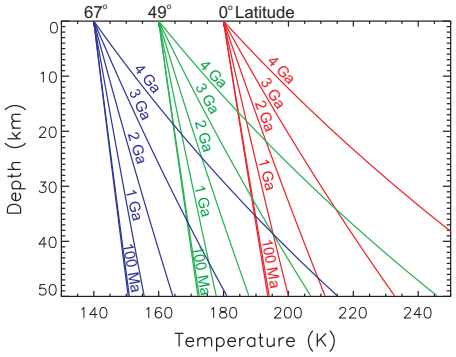

Fig. 3. Temperature in the ice layer (i.e., $T(z)$, Eq. (4)) through time for surface temperatures of 180 K (red), 160 K (green), and 140 K (blue) (latitudes of 0°, 49°, and 67°, respectively, see Fig. 4). Times are indicated on each profile. The profiles at 100 Ma and 10 Ma lie on top of each other for each surface temperature due to their nearly identical heat fluxes. (For interpretation of the references to color in this figure legend, the reader is referred to the web version of this article.)

$$T_s = \left[\frac{(1-A)F_c}{\epsilon\sigma}\frac{\sin\theta}{\pi}\right]^{\frac{1}{4}}, \quad (5)$$

for θ less than Ceres' obliquity, where A is Ceres' bolometric albedo, ϵ is the emissivity (assumed to be 0.9), $\sigma = 5.67 \times 10^{-8}$ W m^{-2} K^{-4} is the Stefan–Boltzmann constant, and F_c is the solar flux at $a = 2.77$ AU ($F_c = F_\odot/a^2 = 179$ W m^{-2}, where $F_\odot = 1370$ W m^{-2} is the solar constant). Ceres' bolometric albedo is so far undetermined. Ceres' measured geometric albedos (which may be greater or less than the bolometric albedo) range from 0.07 to 0.1 in the visible (Millis et al., 1987; Tedesco, 1989) and from 0.04 to 0.09 in the UV (Li et al., 2006). We use a conservative value of 0.1 for the bolometric albedo. A lower albedo would result in warmer surface temperatures and increased viscous relaxation. We assume here that Ceres' obliquity is close to zero (Drummond et al., 1998; Thomas et al., 2005). A higher obliquity (e.g. Bills and Nimmo, 2011) would result in warmer surface temperatures (~90 K) near the poles, but the surface temperatures discussed below would be unaffected.

The resulting global temperature distribution is shown in Fig. 4. The maximum (subsurface average) temperature is 178 K at Ceres' equator. Temperatures decrease slowly across the mid-latitudes, decreasing to 160 K at ±49°, and 140 K at ±67°. Temperatures can theoretically drop below 100 K at very high latitudes ($\geqslant$84°), but uncertainties in Ceres' obliquity (Eq. (5) is only valid at co-latitudes greater than the obliquity) and the small surface area encompassed by these latitudes (0.5% of the surface) render evaluation of crater relaxation at such temperatures uninformative. The temperatures derived here are in broad agreement with those derived by Fanale and Salvail (1989), who found a maximum equatorial temperature of 180 K. Despite the similar approach to that described here, the latitudinal profile of surface temperature shown in their Fig. 1 deviates modestly from the expected $\cos^{\frac{1}{4}}\theta$ dependence on co-latitude, resulting in somewhat higher temperatures in their study. Our diurnally-averaged temperatures are substantially less than both the maximum measured and theoretical temperatures for a surface in instantaneous radiative equilibrium ($T_{max} = 235$ K, Saint-Pe et al., 1993), but are more meaningful for Ceres' subsurface (i.e., below the thermal skin depth) and longer timescales. Finally, we note that the temperatures described here do not account for the insulating effects of the silicate regolith, which could result in even higher lithospheric (i.e., sub-regolith) temperatures and greater relaxation rates.

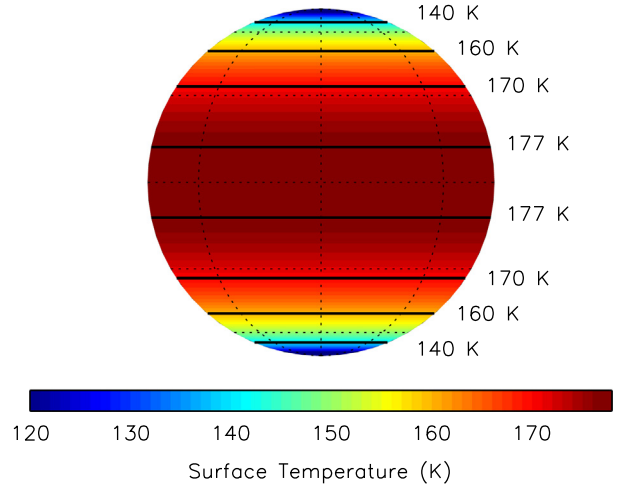

Fig. 4. Color map of theoretically-derived surface temperatures on Ceres. The maximum temperature is 177 K at the equator. Temperatures of 160 K and 140 K occur at latitudes of 49° and 67°, respectively. (For interpretation of the references to color in this figure legend, the reader is referred to the web version of this article.)

3.3. Modeling approach

For each crater shape, we simulate viscous relaxation at three surface temperatures: 180 K, 160 K, and 140 K. These temperatures are representative of Ceres' equatorial, middle, and polar latitudes (see above). For each crater shape and surface temperature combination, we investigate relaxation of both ancient and recent craters by examining four different crater ages (i.e., formation times): 10 Ma, 100 Ma, 1 Ga, and 4 Ga. Fig. 3 shows the simulated temperature profiles in the ice shell through time (calculated by combining the surface temperatures above and the time-varying heat fluxes described in Section 3.1) for each of the latitudes (i.e., surface temperatures) investigated. Ancient craters (4 Ga) not only have much longer timescales over which relaxation can occur, but the higher ancient heat flux leads to higher ice temperatures at depth. Even in the polar regions, deep ice exceeds 200 K, permitting relatively rapid relaxation of large craters (which "feel" the low-viscosity ice at depth). In contrast, recent craters have had only a short time to relax, and the lower heat fluxes result in relatively cold ice throughout the layer. For craters that formed within the last 100 Ma, the temperature of the ice increases by only 10 K over a depth of 50 km. This cold, high-viscosity ice retards relaxation in Ceres' polar regions.

4. Predicted crater morphologies

4.1. Viscous relaxation in a pure ice layer

The degree of viscous relaxation on Ceres depends strongly on the surface temperature. Fig. 5 shows the predicted present-day crater topography for three different crater diameters (4 km, 12 km, 20 km), and Fig. 6 indicates the predicted present-day degree of relaxation (as a percentage of the initial apparent crater depth), apparent crater depths (i.e., the depth relative to the ground plain, rather than the rim), and rim heights as a function of crater diameter, crater age, and latitude (surface temperature). At equatorial latitudes ($T_s = 180$ K), extensive topographic relaxation will occur. All craters greater than 4 km in diameter that are at least 100 Ma old will be completely relaxed at present (Fig. 6). Young, small craters (i.e., those formed within the last 10 Ma), will appear mostly relaxed: a 4-km diameter crater will be relaxed by more than 80%.

At such warm temperatures complete crater erasure is plausible. As mentioned above, viscous relaxation timescales are a function of topographic wavelength. Thus, short-wavelength rims are often preserved, allowing identification of even highly relaxed craters (e.g., the highly relaxed craters on Enceladus (Bland et al., 2012)). In contrast, Fig. 5 demonstrates that craters in Ceres' warm equatorial region ($T_s = 180$ K) can become so relaxed that nearly all the topography is removed. Fig. 6 indicates that crater depths are reduced to 10–50 m (depending on the crater diameter) in craters as young as 100 Ma old (and older). Rim heights are reduced to 30 m or less in these same craters (the 20 km crater shown in Fig. 5 has no measurable rim). For craters 1 Ga old, nearly complete erasure might be expected. These results, therefore, predict that crater densities in Ceres' equatorial region are much lower than would be expected for a rocky body (plausibly near zero).

Intriguingly, the rapid relaxation of impact craters in Ceres' equatorial region may provide insight into the recent cratering rate in the asteroid belt. Assuming the radiogenic heat flux and surface temperature are well constrained, the relaxation state of each crater (coupled with its diameter) provides a constraint on its age, and thus the modern impactor flux. This contrasts with the icy satellites where uncertainty in tidal heating histories and slower relaxation rates require assuming an impactor flux a priori. The

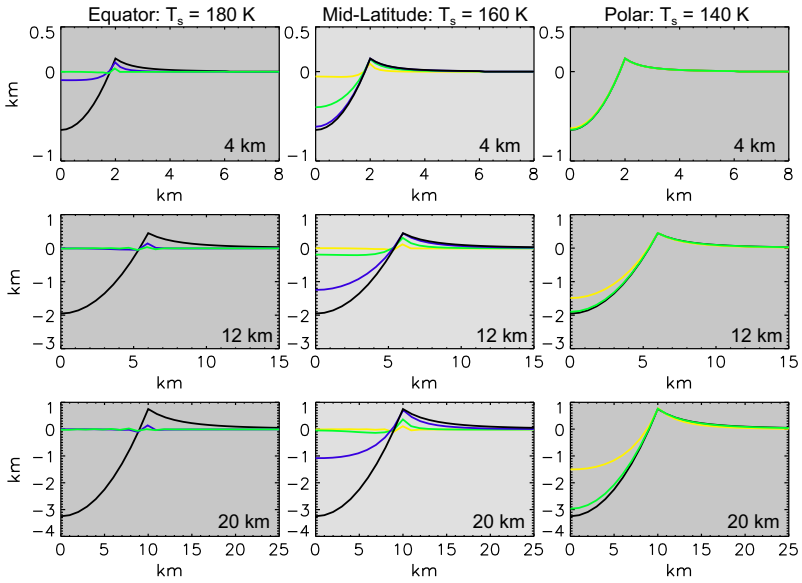

Fig. 5. Profiles of predicted crater morphology for three crater diameters (*top* 4 km, *middle* 12 km, *bottom* 20 km) at equatorial (T_s = 180 K, left), middle (T_s = 160 K, center), and polar (T_s = 140 K, right) latitudes. Black curves show the initial crater topography. Yellow, green, and blue curves show the predicted present-day topography for a 1-Ga old crater, 100-Ma old crater, and 10-Ma old crater, respectively. Note the change in scale for each crater. (For interpretation of the references to color in this figure legend, the reader is referred to the web version of this article.)

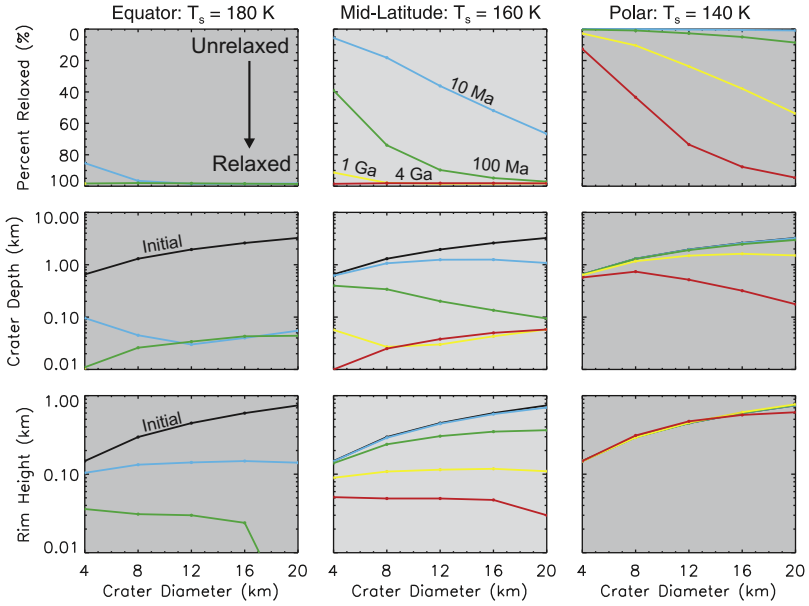

Fig. 6. The percent relaxation (top), apparent crater depth (middle), and rim height (Bottom) in Ceres' equatorial (T_s = 180 K, left), middle (T_s = 160 K, center), and polar (T_s = 140 K, right) latitudes, as a function of crater diameter for four different crater ages: 10 Ma (blue), 100 Ma (green), 1 Ga (yellow), and 4 Ga (red). Curves are also labeled. Black curves indicate initial crater depths and rim heights. Note the log scale in the middle and bottom rows. (For interpretation of the references to color in this figure legend, the reader is referred to the web version of this article.)

plausibility of such an investigation on Ceres may depend on a better understanding of the grain size and particulate content of the ice layer (see Sections 4.2 and 4.3.1), and whether sufficient craters exist at equatorial latitudes to provide meaningful statistics.

At Ceres' mid latitudes, where temperatures are modestly cooler (T_s = 160 K), topographic relaxation is still expected to be extensive. Figs. 5 and 6 indicate that craters older than ~1 Ga will be completely or nearly–completely relaxed at present. Craters 20 km in diameter or larger should be substantially relaxed (60% or greater) even if they are relatively young. Smaller, more recent craters will be only partially relaxed (~40% for a 100-Ma old, 4-km diameter crater). These craters may even appear relatively deep (e.g., 400 m for the 100-Ma old, 4-km diameter crater, Fig. 5), but will be shallower than expected from depth-diameter scaling. Crater erasure is unlikely in these regions, as significant crater depths and rim heights (100 m or more) are preserved (Figs. 5 and 6). Thus, whereas crater morphology will be strongly affected, crater densities likely will not be (i.e., even completely relaxed craters will have intact, observable rims). Notably, 75% of Ceres' surface has diurnally averaged temperatures of 160 K or greater (i.e., is between ±49° latitude), suggesting that pristine craters will generally be rare across most of Ceres' surface.

Several large albedo features have already been identified on Ceres. In particular, Carry et al. (2008) tentatively categorized several features in Ceres' mid-latitudes (near 30°N) as impact structures with diameters of 180 km or more. The surface

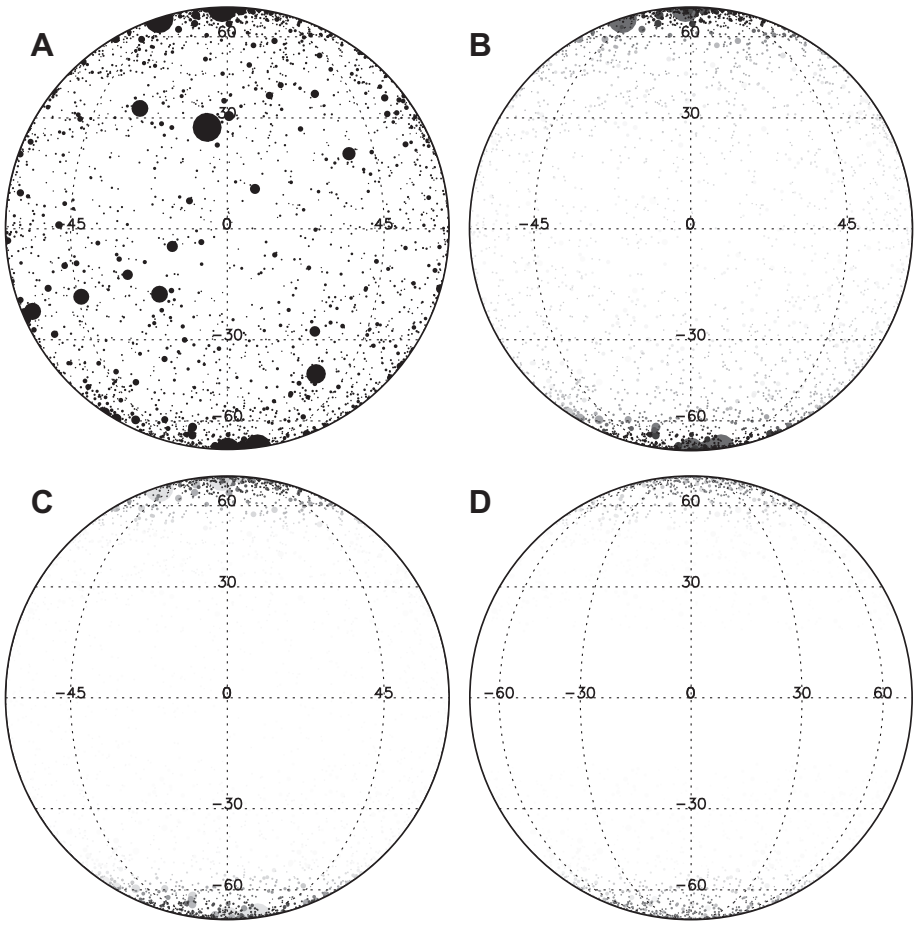

Fig. 7. Orthographic maps of crater preservation on Ceres. (A) The initial crater distribution. Crater longitudes and latitudes were randomly generated, and the size-frequency distribution was derived from that of de Elía and di Sisto (2011). The maximum crater diameter is 100 km. (B) The same crater distribution as in A, but shaded to reflect the predicted *current* relaxation state of 100 Ma old craters (black = fresh, white = completely relaxed). Relaxation states were derived from the simulations shown in Fig. 6 using bilinear interpolation. (C) and (D) are as in (B), but for crater ages of 1 Ga and 4 Ga, respectively.

temperature in this region is likely to be near 170 K (see Fig. 4). Given the warm surface temperatures and the large diameters of these features we suggest that, if these features are indeed impact related, they will be extremely relaxed. Morphologically they are therefore likely to resemble palimpsest features on the icy satellites Ganymede and Callisto (though palimpsests may differ in their formation). Palimpsests typically have low relief (if any) and are identified primarily as an albedo anomaly (e.g. Jones et al., 2003).

At polar-like temperatures of T_s = 140 K (latitudes $\geqslant 67°$, comprising 8% of Ceres' surface), substantially less viscous relaxation is expected. While the surface temperature may exceed those of most icy satellites (many of which display evidence of viscous relaxation), Ceres' low radiogenic heat flux precludes extensive relaxation. The largest and oldest craters may show evidence of relaxation (Figs. 5 and 6): a 1-Ga old, and a 4-Ga old, 20-km diameter crater will have relaxed by ~50% and >90% at present, respectively. Smaller craters are expected to show very little viscous relaxation (a 4-km diameter crater essentially does not relax at all). Crater rims are preserved at all crater sizes. Because of their better preservation state, Ceres' polar craters will be most useful for analyzing depth-diameter ratios and simple-complex transition diameters.

The results of our relaxation simulations are summarized in Fig. 7, which shows the spatial distribution of crater retention on Ceres for craters with ages of 4 Ga, 1 Ga, and 100 Ma. The craters were randomly distributed in latitude and longitude, and the initial size frequency distribution was derived from the crater distribution of de Elía and di Sisto (2011). For clarity, the total number of craters plotted have been decreased by an order of magnitude relative to their results, and the maximum crater size was limited to 100 km. The crater distribution shown here is only intended to be an approximate representation of Ceres' expected crater distribution, and no attempt was made to modify the crater density as a function of time (i.e., the same initial distribution was used in each panel, neglecting the t^{-1} dependence on cratering rate with time). Despite these simplifications, the dramatic effect of viscous relaxation is clearly illustrated. As described above, Ceres' equatorial latitudes are expected to be deficient in craters of all sizes. Even craters formed within the last 100 Ma are nearly completely relaxed. At high latitudes, only the smallest craters are preserved for 4 Ga. Large craters can be preserved only at the highest latitudes, and only if formed within the last ~1 Ga. The rapid relaxation of even recently formed craters in equatorial- and mid-latitudes results in similar crater retention maps for each crater age (especially for 4 Ga old and 1 Ga old craters). Only the polar regions, where the cold temperatures inhibit relaxation, show substantial variation in the relaxation state of different aged craters.

4.2. Effect of ice grain size

As discussed in Section 3 the grain size of ice in the interior of a planetary body (e.g., an icy satellite or Ceres) is poorly constrained. Because both diffusion creep and grain boundary sliding rheological mechanisms are dependent on grain size (m = 2 and 1.4 in Eq. (3), respectfully) the assumed grain size can have a powerful

influence on model results (e.g. Bland and McKinnon, 2012a). Reasonable grain size estimates vary from 100 μm to a centimeter or more, depending on the temperature and stress state of the ice, and ice grain sizes are likely to vary both spatially and temporally (e.g., Barr and McKinnon, 2007).

The effect of ice grain size on our viscous relaxation calculations is illustrated in Fig. 8 for 1-Ga old, 4 km and 20 km diameter craters. Increasing the ice grain size increases the effective viscosity of the ice, and thus increases the timescale for viscous relaxation across Ceres (i.e., at every surface temperature). For craters 20 km or larger, however, the ice grain size has a negligible effect at Ceres' equator and mid-latitudes. Only in the poles is crater relaxation substantially retarded, decreasing from ~50% relaxed to ~5% relaxed for an order of magnitude increase in grain size (1–10 mm). Thus, if Ceres' ice is large grained, moderate to large diameter craters will be better preserved at the poles.

For smaller craters (4-km diameter), the assumed grain size has a larger effect. At the equator, relaxation of a 1-Ga old crater is again negligibly affected by an increase in grain size (though younger craters may appear less relaxed). Grain size also generally has a negligible affect in the polar regions. Whereas the relaxation state decreases by more than an order of magnitude (from 3% to 0.1%), polar craters in this size range will appear pristine in either case. It is in Ceres' mid-latitudes that grain size may have an appreciable effect. There, increasing the grain size by an order of magnitude reduces the predicted current relaxation state of a 1-Ga old crater from 90% to 20%. Thus craters that were nearly completely relaxed at smaller grain sizes are only slightly relaxed at large grain sizes.

In summary, if the ice grain size in Ceres' interior is significantly larger than assumed in our nominal simulations crater preservation will be better at the poles, even for relatively large craters. Large ($\geqslant$20 km diameter) craters at mid-latitudes will still be highly relaxed but smaller craters will be preserved with little viscous relaxation. All craters will still appear highly relaxed in the equatorial region, except perhaps relatively young craters. Alternatively, if the ice grain size on Ceres is smaller (say 100 μm) the effective viscosity of the ice will be lower, and even craters in Ceres' polar regions will undergo substantial relaxation.

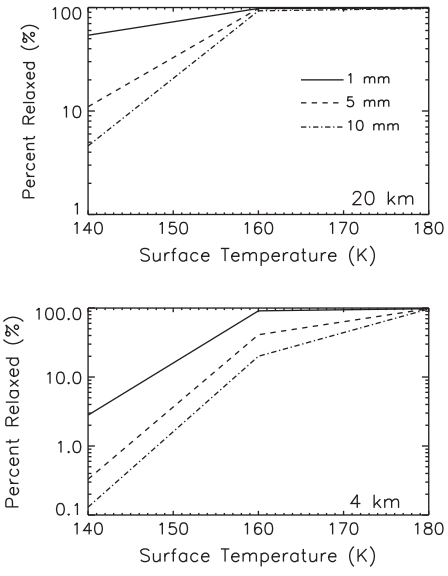

Fig. 8. The range of plausible relaxation states for a 1-Ga old, 20-km (top) and 4-km (bottom) diameter crater as a function of surface temperature and ice grain size (pure ice layer). The solid, dashed, and dot-dashed curves correspond to grain sizes of 1 mm, 5 mm, and 10 mm, respectively. Note the change in log scale between the top and bottom panels.

4.3. Effects of near-surface composition and structure

The results described above demonstrate that extensive viscous relaxation is expected for our nominal case of a thick, homogeneous, near-surface, pure ice I layer (i.e., no thick overlying crust). While this simple set of conditions is plausible, the actual conditions on Ceres may be more complex. Below we discuss the effects of such complexity. None of these complications profoundly changes our basic conclusion that impact craters (or other long-wavelength topography) will rapidly viscously relax in Ceres' equatorial- and mid-latitudes.

4.3.1. Composition of Ceres' crust

The simulations described in Section 4 assume that Ceres' "crust" and deeper ice are both composed of pure water ice. This assumption is consistent with thermal–physical models of Ceres' structural and thermal evolution. Castillo-Rogez and McCord (2010) argue that, if Ceres formed shortly after the formation of CAI's, then short-lived radiogenic heating is sufficient to completely melt the body, leaving a pure water ice surface layer. If Ceres formed later, a dirty ice layer tens of kilometers thick remains after formation (e.g., McCord and Sotin, 2005). Such a mixed ice/rock layer would be gravitationally unstable, and might be easily disrupted during the late heavy bombardment (McCord and Sotin, 2005; Castillo-Rogez and McCord, 2010). Alternatively, the melting and refreezing of Ceres' ice, and/or the hydration, and possibly dehydration, of Ceres' silicate material would result in a complex sequence of large-scale volume changes that might have resulted in disruption of Ceres' crust (McCord and Sotin, 2005). In either case, foundering of the mixed ice/rock crust would result in a more-or-less pure ice-I, near-surface layer on Ceres.

Yet Ceres' surface is clearly composed of "rocky" material (Rivkin et al., 2011). If this rocky layer formed as a surface lag as water ice sublimated away (e.g., Fanale and Salvail, 1989; Schorghofer, 2008), then some particulate non-ice material must be present within the ice layer. Whether this material is mixed throughout the putative ice layer (which could affect the ice rheology), or simply resides in an unconsolidated near surface regolith (which would not affect the rheology) is undetermined. The latter case is more consistent with models of Ceres' evolution (Castillo-Rogez and McCord, 2010), but we note that the Solar System contains a number of bodies in which separation or ice and rock is far from complete (e.g., Callisto (Anderson et al., 2001) and possibly Titan (Bland and McKinnon, 2012b)). Given the uncertainty in the composition of Ceres' near surface ice we simulate the viscous relaxation of crater topography in a homogeneous mixed ice/rock layer. These simulations are representative of the case where the thickness (L_c) of the "crust" (i.e., the mixed layer) is greater than the diameter of the crater (i.e., $L_c \gtrsim D$). The effect of a "thin" crust (i.e., $L_c \ll D$) is discussed in Section 4.3.2.

The rheology of ice and rock mixtures is complex, and depends strongly on both the volume fraction of particles (ϕ) and the dominant rheological mechanism. Durham et al. (1992) found that particulates had only a modest effect on viscosity in the dislocation creep regime ($n = 4$). Whereas volume concentrations of $\phi = 0.4$–0.5 (near the theoretical closest packing limit for equal sized spheres) increased the effective viscosity by two orders of magnitude, smaller concentrations have a smaller effect: a factor of 5–10 increase at $\phi = 0.3$, and only a factor of ~2 increase at $\phi = 0.1$ (Durham and Stern (2001) suggest viscosity increases by a factor of $e^{nb\phi}$, where $b \sim 2$ is experimentally determined). The strength increase is not due to pinning of dislocations but rather a combination of increased tortuosity of flow paths around particles and viscous drag (Durham et al., 1992). The increase in viscosity is generally independent of particulate composition (though see Durham et al., 1992). Studies of mixtures of ice and hydrated magnesium

salts (Meridianiite, $MgSO_4{\cdot}11H_2O$) with ϕ of 0.3–0.5 result in a similar order of magnitude increase in viscosity within the dislocation creep regime (McCarthy et al., 2011). Pathare et al. (2005) have argued that similar viscosity increases should apply to the GBS mechanism as well, though the smaller stress exponent ($n = 1.8$) further reduces the viscosity increase to 1.5–6× pure ice for ϕ of 0.1–0.5, respectively. Theoretical work on the effect of particulates on Newtonian rheology (a deformation mechanism relevant to the relatively low stress regime of crater relaxation) is consistent with the smaller dependence on particulate abundance at small n, and suggests that the viscosity increase in the low-stress regime is a factor of 2–3 for $\phi = 0.3$ and one-to-two orders of magnitude for $\phi = 0.5$ (Einestein, 1906; Roscoe, 1952; Friedson and Stevenson, 1983). A volume fraction of 0.1 increases the viscosity by only a factor of 1.4.

The effect of particulates on the ice viscosity (and hence on the relaxation timescales) is modulated by the increase in the density of the mixed ice/rock layer (see, e.g., Pathare et al., 2005). A layer that is 50% ice (density 930 kg m^{-3}) and 50% dust (3000 kg m^{-3}) by volume would have a density of ≈1970 kg m^{-3}. The factor of two increase in density would (all else being equal) decrease the timescale for relaxation by roughly a factor of two. The effect is smaller if the particulate material is hydrated salts. Meridianiite ($MgSO_4{\cdot}11H_2O$) has a density of only ∼1500 kg m^{-3} so even if present at the 50% level would increase the density by only a third (to ∼1200 kg m^{-3}). In general, the effect of the density increase, which decreases relaxation timescales, is a factor of two or less, whereas the effect of the viscosity increase, which increases relaxation timescales is a factor of two or more.

Because the inclusion of particulates increases the viscosity of ice, it is useful to consider what effect large volume fractions of particulates mixed into Ceres' putative ice layer would have on Ceres' surface topography. Given the uncertainties in the volume fraction of particulates in Ceres' ice layer, the composition of those particulates (i.e., how they affect the layer density), and the actual effect of those particulates on the complex composite rheology of water ice (i.e., with contributions from multiple non-Newtonian and Newtonian flow laws) we take a conservative approach and simulate a range of plausible mixed-layer compositions: an order of magnitude increase in effective viscosity *without* an accompanying density increase (consistent with the effect of 50% hydrated salts on dislocation creep rheology, referred to as Case A); an order of magnitude increase in effective viscosity with a factor of two increase in density (consistent with the effects of 50% silicate dust on dislocation creep rheology, referred to as Case B); and a factor of five increase in viscosity with a ∼50% increase in density (roughly consistent with the effect of 30% dust on composite ice rheology, refereed to as Case C). These sets of conditions include both an upper bound to the viscosity of an ice/rock mixture with a particulate volume fraction near the theoretical maximum for uniform spherical particles (i.e., relatively extreme conditions, Case A), and more physically plausible sets of conditions (Case B and C).

Fig. 9 shows the expected degree of relaxation as a function of crater age for craters with diameters of 20 km and 4 km assuming the near surface layer is a mix of ice and rock (conditions described above). Also shown is the degree of relaxation for the pure ice case. Relaxation of larger craters is only modestly affected by particulates. A young (10 Ma old) 20-km diameter crater at equatorial temperatures ($T_s = 180$ K) will relax by at least 70%, even assuming our most extreme conditions (Case A). A 20-km diameter crater at least 100-Ma old, should be completely relaxed independent of the presence or absence of particulates within the ice layer. At cooler temperatures (i.e., higher latitudes) craters are subsequently less relaxed. At mid-latitudes, the same 100-Ma old, 20-km-diameter crater might relax by as little as 20% if the extreme conditions (Case A) hold, though under more realistic conditions (Case C)

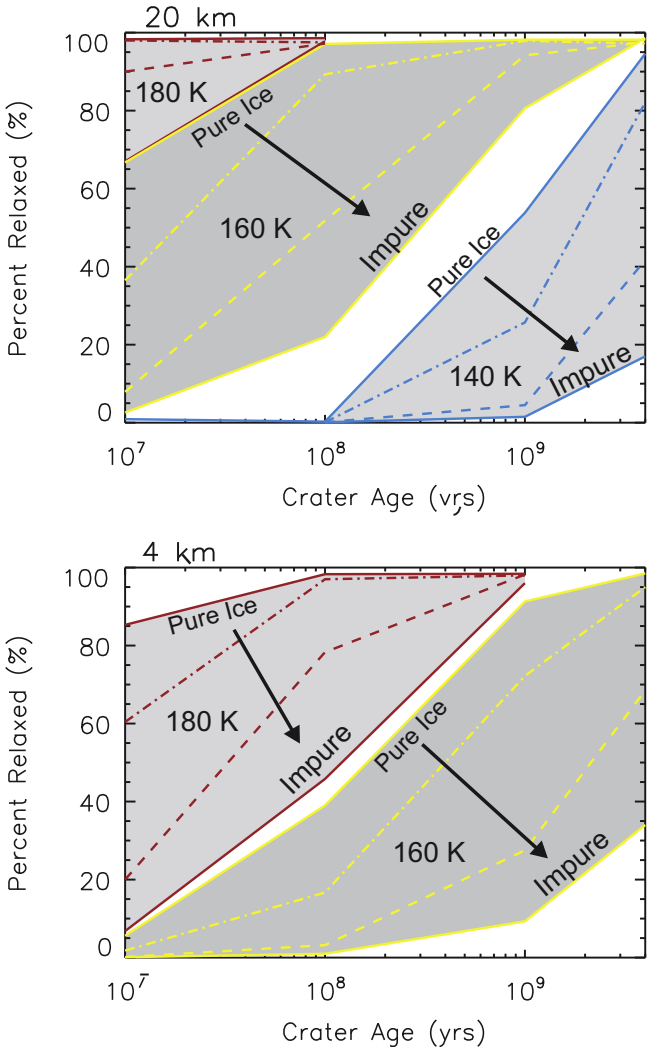

Fig. 9. The range of plausible relaxation states for a 20-km diameter (top) and 4-km diameter (bottom) crater as a function of crater age and particulate volume fraction in the ice layer. The shaded regions bounded by red, yellow, and blue curves correspond to surface temperatures of 180 K, 160 K, and 140 K, respectively. For each set of curves the bottom boundary is set by assuming an order of magnitude increase in ice viscosity (Case A conditions, see text). The upper bound is set by the pure ice end member shown in Fig. 6. The dashed and dot-dashed curves within each shaded region correspond to Case B and Case C conditions as described in the text, respectively. (For interpretation of the references to color in this figure legend, the reader is referred to the web version of this article.)

the relaxation reaches nearly 90%. The oldest craters (⩾1 Ga) will be at least 80% relaxed independent of particulate content. At cold, polar-like temperatures relaxation can be strongly inhibited by particulates, with even 4-Ga old, 20-km diameter craters remaining only slightly relaxed (20%) under Case A conditions, but 80% relaxed under Case C conditions.

Fig. 9 indicates that inclusion of large volume fractions of particulates more strongly inhibits relaxation at small crater sizes. For Case A, a young 4-km diameter crater will relax by less than 10% even at Ceres' warm equator. For older craters (⩾1 Ga) substantial or complete relaxation (∼100%) can occur in Ceres' equatorial region, but under Case A conditions, minimal relaxation occurs at higher latitudes (∼30% after 4 Ga for $T_s = 160$ K). Substantial relaxation results under the more-relaxed conditions of Case B and C (69% and 95% after 4 Ga, respectively). Very little relaxation of small craters occurs in the polar regions even for pure ice (Fig. 6).

We emphasize that relaxation states under the extreme Case A conditions discussed in this section are the *minimum* degree of

relaxation expected assuming Ceres has a near-surface ice layer. They require that Ceres' "ice" layer is composed of nearly 50% low-density particulate material *by volume* to depths of tens of kilometers (i.e., the layer is as much hydrated salt as it is ice). Even with such a conservative assumption, in the equatorial region we still expect nearly complete relaxation of all craters with $D \geqslant 20$ km and all small craters older than ~1 Ga. Only in the mid-latitudes and polar regions do we expect a mixed ice/rock composition to have a pronounced effect on crater morphology, and under the more realistic Case B and C conditions substantial crater relaxation still occurs across Ceres. The fact that crater morphology is affected by the compositions of the ice layer (particulate fraction and density) can in itself provide insight into the composition of Ceres' ice. If, for example, *Dawn* observes mid-sized craters (e.g., 20-km diameter) in Ceres' mid-latitudes that are only partially relaxed it might indicate that Ceres' "ice layer" is actually a mixed ice/rock layer (see Section 5).

4.3.2. Thickness of Ceres' crust

In Section 4.3.1 we described the effect of ice layer composition on crater relaxation assuming a thick (tens of kilometers) homogeneous layer. Here we discuss the effects of a two layer near-surface structure consisting of a relatively thin, high-viscosity mixed ice/rock layer (the "crust") overlying pure ice. Such would be the case if melting and differentiation failed to completely melt the outermost portion of Ceres (e.g., McCord and Sotin, 2005) and this high-viscosity, high-density carapace avoided foundering over Solar System history. For simplicity we assume that the viscosity of the crust is an order of magnitude greater than that of pure ice and neglect the increase in density associated with large dust fractions (i.e., Case A above). Note that this "crust" is distinct from any unconsolidated surface regolith layer (e.g., a sublimation lag), which would not effect the mechanical properties of the underlying intact layer.

Fig. 10 illustrates the effects of the high-viscosity crust on 1-Ga old craters in Ceres' mid-latitudes. In general, crater relaxation is unaffected by the presence of a high-viscosity layer that is a small fraction of the crater radius. The relaxation states of a 20-km diameter crater are indistinguishable in the presence of a high-viscosity crust up to 5 km thick. Only once the crust becomes comparable to the crater radius (e.g., 10 km and 5 km for the 20-km and 12-km diameter craters, respectively) does it begin to influence the relaxation, and even then viscous relaxation is retarded less then in the case of a homogeneous high-viscosity layer (Fig. 9). Once the crustal thickness is comparable to the crater diameter the results are generally indistinguishable from the case of a homogeneous mixed ice/rock layer.

If Ceres' (putative) crust is 20 km thick, we expect craters 20 km in diameter and smaller to be affected by its presence while large craters are less effected. Craters larger than ~40 km are unlikely to be affected at all. Thinner crusts would affect commensurately smaller craters whereas thicker crusts would affect larger ones. The relaxation states shown in Fig. 10 are for the extreme conditions (Case A) described in Section 4.3.1. More realistic conditions would result in similar, though smaller, effects. In principle, the size dependence of the effect of the high-viscosity crust on crater relaxation might permit determination of Ceres' crustal thickness, though untangling these effects from those of surface temperature, composition, grain size, lateral heterogeneities, and the normal wavelength dependence of viscous relaxation could prove challenging.

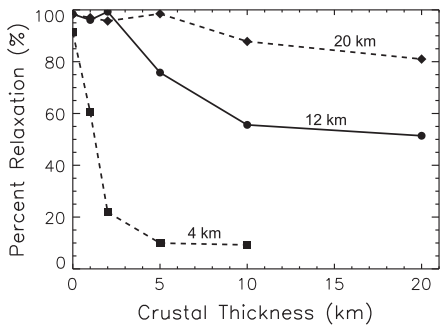

Fig. 10. The effect of a near-surface high-viscosity mixed ice/rock "crust" on the predicted relaxation state of 1 Ga year old craters in Ceres' mid-latitudes (T_s = 160 K). The dashed/square, solid/circle, and dash-dot/diamond curves correspond to crater diameters of 4 km, 12 km, and 20 km, respectively.

4.3.3. Thickness of the ice layer

The internal structure of Ceres is such that the putative ice layer may be relatively thin and underlain by a strong substrate (i.e., the rocky core). Parmentier and Head (1981) have shown, using a Newtonian ice rheology, that the presence of a rigid substrate can have a pronounced effect on the morphology of relaxed craters when the thickness of the viscous layer (L_i) is substantially less then the crater diameter ($L_i/D \leqslant 0.15$) (see also Pathare et al., 2005). Based on this result, for a 20-km diameter crater, Ceres' ice layer would have to be less than 3 km thick before the crater relaxation process is grossly affected. Our simulations agree with this general conclusion. In our standard domain the thickness of the viscous layer is 2.5× the crater diameter (i.e., 5× the crater radius). For a 100-Ma old, 20-km diameter crater at a surface temperature of 160 K, decreasing the domain depth from 50 km (the nominal depth, $L_i/D = 2.5$) to 20 km (i.e., $L_i/D = 1$) resulted in only a 0.3% reduction in the percent relaxation (from 97.1% to 96.8%). Even decreasing the viscous layer thickness to 10 km ($L_i/D = 0.5$) results in a negligible change in relaxation state. In short, none of the craters described here are likely to be influenced by the rocky core unless the ice layer is much less than 10 km thick.

Larger craters on Ceres could, however, be affected by the presence of the rigid core. If the ice layer is very thin (say 20 km) a 200-km diameter crater would have an L_i/D ratio of 0.1, resulting in relatively rapid relaxation of the long-wavelength portions of the rim and retarded relaxation of the long-wavelength portions of the crater bowl (Parmentier and Head, 1981). Alternatively, if the ice layer is thick (say 80 km), L_i/D for the same crater would be 0.4, and the crater should exhibit the canonical relaxed morphology. Careful modeling of the relaxation of such large craters (they will also be strongly affected by Ceres' radius of curvature – a 200-km diameter craters spans ~25° of latitude) may therefore provide constraints on the thickness of Ceres' ice layer by constraining L_i/D. The dynamical modeling of de Elía and di Sisto (2011) suggests that Ceres should have ~30 craters with $D \geqslant 200$ km, though such large craters may not be retained over Ceres' history (see Fig. 7). Such modeling is beyond the scope of the present work.

4.3.4. Compositional heterogeneity

In addition to the complexities discussed above, Ceres' near surface structure is likely to be both laterally and radially heterogenous. In particular, the vagaries of differentiation and early evolution of the dwarf-planet might have resulted in compositional or grain size differences due to incomplete compositional mixing, frozen compositionally-driven diapirs, or localized hydrothermal activity in the silicate core (e.g., hydration or dehydration). Additionally, incomplete foundering of a primordial "crust" (due to localized tectonics or impacts) could have resulted in lateral crustal thickness variations. Yet, as demonstrated throughout Section 4.3, for reasonable conditions, Ceres' surface temperature is the primary influence on the rate of viscous relaxation. The basic latitudinal dependence of crater morphology predicted here is

therefore relatively robust to lateral variations in Ceres' internal structure.

5. Dawn observations: probing Ceres' internal structure

The morphology of Ceres' impact craters provides direct insight into the internal structure of the dwarf planet. Below we summarize specific observations of Ceres' craters that the *Dawn* spacecraft can make (requiring both imaging and topography) to constrain Ceres' internal structure.

5.1. Global

The basic morphology (i.e., relaxation state) of Ceres' craters alone can constrain whether the expected thick ice layer (e.g., McCord and Sotin, 2005; Thomas et al., 2005; Castillo-Rogez and McCord, 2010, and many others) actually exists in Ceres' near-surface. The viscous relaxation study discussed here is predicated on the existence of such an ice layer. We have shown that, given the existence of an ice layer, extensive viscous relaxation of impact craters is unavoidable in Ceres' equatorial and middle latitudes. This result is largely independent of ice grain size, particulate content, the presence of a high-viscosity "crust," or the thickness of the ice layer. If Ceres does not contain an ice layer (e.g., Zolotov, 2009), then crater morphologies and crater densities should largely be unmodified. Thus, we expect that the first moderate resolution images of Ceres returned by the *Dawn* mission (better than say 1 km/pixel) will confirm or refute the existence of Ceres' expected ice layer. Determination of the simple-to-complex transition diameter provides an additional constraint on Ceres' basic internal composition.

5.2. The equatorial region

If Ceres contains significant quantities of ice (i.e., 50% or more by volume) to depths of tens of kilometers, then craters of all sizes will be relaxed in the equatorial region. Low crater densities (i.e., due to complete crater erasure, as opposed to highly relaxed but identifiable craters) would suggest relatively compositionally pure ice and/or the lack of a thick high-viscosity "crust." Alternatively, if small craters (4-km diameter) are only moderately relaxed it suggests the presence of large volume fractions of non-ice material. Note that large ice grain sizes cannot inhibit relaxation in the equatorial region, providing a mechanism for distinguishing the effects of grain size and particulate abundance. If equatorial craters are pristine it strongly indicates a lack of subsurface ice on Ceres.

5.3. The mid-latitudes

If Ceres contains a relatively pure ice layer, moderate and large craters in Ceres' mid latitudes will appear relaxed, whereas small craters ($\sim$4 km diameter) will be unrelaxed or only partially relaxed. The greater the particulate content and the larger the grain size of the ice, the less relaxed mid-sized craters will appear. If crater morphologies in the equatorial region suggest Ceres' subsurface ice is relatively free of contaminants but craters at mid-latitudes are relatively pristine, then it suggests that Ceres' ice is relatively large grained. A careful survey of spatial variations in relaxation states and crater size might permit constraining the location and thickness of any remaining high-viscosity crust. However, deconvolving the effects of ice contaminants, grain size, and crustal thickness in Ceres' mid-latitudes may require a more focused modeling effort.

5.4. The polar regions

Ceres polar regions are expected to retain large numbers of small craters, and even relatively large craters (20 km diameter) will appear only moderately relaxed. Because relaxation is strongly inhibited by the cold polar temperatures, the region is less useful for constraining Ceres' internal structure. The better preservation state of polar craters, however, makes them useful for understanding Ceres cratering flux, depth-to-diameter relationships, and simple-to-complex transitions. Additionally, if *Dawn* images *do* reveal small, highly-relaxed craters in the polar regions of Ceres it suggests that the body may have undergone some degree of true polar wander in its past. Such true polar wander would require the decoupling of the ice layer from the rocky core by a liquid water layer (a condition permitted in some thermal evolution scenarios (McCord and Sotin, 2005; Castillo-Rogez and McCord, 2010)), and could result from the existence of a thicker ice layer in the cold polar region due to the colder surface temperatures (cf. Mohit et al., 2012). Thus, Ceres' polar craters may provide clues to the past and/or current existence of internal liquid water layers within the dwarf-planet.

Acknowledgments

MTB thanks K.N. Singer for many useful discussions regarding nearly every aspect of this manuscript, W.B. McKinnon for comments that greatly improved the paper, and J.P. Emery for discussions of Ceres' composition. Tom McCord and Asmin Pathare provided insightful reviews. This work was supported by NASA Planetary Geology and Geophysics Program NNX11AP16G.

References

A'Hearn, M.F., Feldman, P.D., 1992. Water vaporization on Ceres. Icarus 98, 54–60. http://dx.doi.org/10.1016/0019-1035(92)90206-M.

Anderson, J.D., Jacobson, R.A., McElrath, T.P., Moore, W.B., Schubert, G., Thomas, P.C., 2001. Shape, mean radius, gravity field, and interior structure of Callisto. Icarus 153, 157–161. http://dx.doi.org/10.1006/icar.2001.6664.

Barr, A.C., McKinnon, W.B., 2007. Convection in ice I shells and mantles with self-consistent grain size. J. Geophys. Res. 112, E02012. http://dx.doi.org/10.1029/2006JE002781.

Barr, A.C., Pappalardo, R.T., 2005. Onset of convection in the icy Galilean satellites: Influence of rheology. J. Geophys. Res. 110, E12005. http://dx.doi.org/10.1029/2004JE002371.

Bills, B.G., Nimmo, F., 2011. Forced obliquities and moments of inertia of Ceres and Vesta. Icarus 213, 496–509. http://dx.doi.org/10.1016/j.icarus.2010.09.002.

Bland, M.T., McKinnon, W.B., 2012a. Forming Europa's folds: Strain requirements for the production of large-amplitude deformation. Icarus 221, 694–709. http://dx.doi.org/10.1016/j.icarus.2012.08.029.

Bland, M.T., McKinnon, W.B., 2012b. Thermal and structural evolution of a partially differentiated Titan. In: AAS DPS Meeting, vol. 44, p. #201.04.

Bland, M.T., McKinnon, W.B., 2013. Does folding accommodate Europa's contractional strain? The effect of surface temperature on fold formation in ice lithosphere. Geophys. Res. Lett.. http://dx.doi.org/10.1002/grl.50506.

Bland, M.T., Singer, K.N., McKinnon, W.B., Schenk, P.M., 2012. Enceladus' extreme heat flux as revealed by its relaxed craters. Geophys. Res. Lett. 39, 17204. http://dx.doi.org/10.1029/2012GL052736.

Carry, B. et al., 2008. Near-infrared mapping and physical properties of the dwarf-planet Ceres. Astron. Astrophys. 478, 235–244. http://dx.doi.org/10.1051/0004-6361:20078166.

Carry, B., Vernazza, P., Dumas, C., Merline, W.J., Mousis, O., Rousselot, P., Jehin, E., Manfroid, J., Fulchignoni, M., Zucconi, J.-M., 2012. The remarkable surface homogeneity of the Dawn mission target (1) Ceres. Icarus 217, 20–26. http://dx.doi.org/10.1016/j.icarus.2011.10.015.

Castillo-Rogez, J.C., 2011. Ceres – Neither a porous nor salty ball. Icarus 215, 599–602. http://dx.doi.org/10.1016/j.icarus.2011.08.007.

Castillo-Rogez, J.C., Conrad, P.G., 2010. Habitability potential of Ceres, a warm icy body in the Asteroid Belt. Astrobiol. Sci. Conf. 1538, #5302.

Castillo-Rogez, J.C., McCord, T.B., 2010. Ceres' evolution and present state constrained by shape data. Icarus 205, 443–459. http://dx.doi.org/10.1016/j.icarus.2009.04.008.

de Elía, G.C., di Sisto, R.P., 2011. Impactor flux and cratering on Ceres and Vesta: Implications for the early Solar System. Astron. Astrophys. 534, A129. http://dx.doi.org/10.1051/0004-6361/201117543.

Dombard, A.J., McKinnon, W.B., 2006. Elastoviscoplastic relaxation of impact crater topography with application to Ganymede and Callisto. J. Geophys. Res. 111, E01001. http://dx.doi.org/10.1029/2005JE002445.

Drummond, J.D., Fugate, R.Q., Christou, J.C., Hege, E.K., 1998. Full adaptive optics images of asteroids Ceres and Vesta; Rotational poles and triaxial ellipsoid dimensions. Icarus 132, 80–99. http://dx.doi.org/10.1006/icar.1997.5882.

Durham, W.B., Stern, L.A., 2001. Rheological properties of water ice: Applications to satellites of the outer planets. Ann. Rev. Earth Planet. Sci. 29, 295–330. http://dx.doi.org/10.1146/annurev.earth.29.1.295.

Durham, W.B., Kirby, S.H., Stern, L.A., 1992. Effects of dispersed particulates on the rheology of water ice at planetary conditions. J. Geophys. Res. 97, 20883–20897. http://dx.doi.org/10.1029/92JE02326.

Durham, W.B., Kirby, S.H., Stern, L.A., 1997. Creep of water ices at planetary conditions: A compilation. J. Geophys. Res. 102, 16293–16302. http://dx.doi.org/10.1029/97JE00916.

Durham, W.B., Prieto-Ballesteros, O., Goldsby, D.L., Kargel, J.S., 2010. Rheological and thermal properties of icy materials. Space Sci. Rev. 153, 273–298. http://dx.doi.org/10.1007/s11214-009-9619-1.

Einestein, A., 1906. Eine neue bestimmung der molekuldimensionen. Ann. Physik. 19, 289–306.

Fanale, F.P., Salvail, J.R., 1989. The water regime of Asteroid (1) Ceres. Icarus 82, 97–110. http://dx.doi.org/10.1016/0019-1035(89)90026-2.

Friedson, A.J., Stevenson, D.J., 1983. Viscosity of rock–ice mixtures and applications to the evolution of icy satellites. Icarus 56, 1–14. http://dx.doi.org/10.1016/0019-1035(83)90124-0.

Gammon, P.H., Klefte, H., Clouter, M.J., 1983. Elastic constants of ice samples by Brillouin spectroscopy. J. Phys. Chem. 87, 4025–4029.

Goldsby, D.L., Kohlstedt, D.L., 2001. Superplastic deformation of ice: Experimental observations. J. Geophys. Res. 106, 11017–11030. http://dx.doi.org/10.1029/2000JB900336.

Johnson, T.V., McGetchin, T.R., 1973. Topography on satellite surfaces and the shape of asteroids. Icarus 18, 612–620. http://dx.doi.org/10.1016/0019-1035(73)90064-X.

Jones, K.B., Head, J.W., Pappalardo, R.T., Moore, J.M., 2003. Morphology and origin of palimpsests on Ganymede based on Galileo observations. Icarus 164, 197–212. http://dx.doi.org/10.1016/S0019-1035(03)00128-3.

Kirby, S.H., Durham, W.B., Beeman, M.L., Heard, H.C., Daley, M.A., 1987. Inelastic properties of ice I_h at low temperatures and high pressures. J. Phys. 48, 227–232.

Lebofsky, L.A., 1978. Asteroid 1 Ceres – Evidence for water of hydration. Mon. Not. R. Astron. Soc. 182, 17P–21P.

Lebofsky, L.A., Feierberg, M.A., Tokunaga, A.T., Larson, H.P., Johnson, J.R., 1981. The 1.7- to 4.2-micron spectrum of asteroid 1 Ceres – Evidence for structural water in clay minerals. Icarus 48, 453–459. http://dx.doi.org/10.1016/0019-1035(81)90055-5.

Li, J.-Y., McFadden, L.A., Parker, J.W., Young, E.F., Stern, S.A., Thomas, P.C., Russell, C.T., Sykes, M.V., 2006. Photometric analysis of 1 Ceres and surface mapping from HST observations. Icarus 182, 143–160. http://dx.doi.org/10.1016/j.icarus.2005.12.012.

Lodders, K., Fegley, B., 1998. The Planetary Scientist's Companion. Oxford University Press, New York.

McCarthy, C., Cooper, R.F., Goldsby, D.L., Durham, W.B., Kirby, S.H., 2011. Transient and steady state creep response of ice I and magnesium sulfate hydrate eutectic aggregates. J. Geophys. Res. 116, E04007. http://dx.doi.org/10.1029/2010JE003689.

McCord, T.B., Sotin, C., 2005. Ceres: Evolution and current state. J. Geophys. Res. 110, E05009. http://dx.doi.org/10.1029/2004JE002244.

McCord, T.B., McFadden, L.A., Russell, C.T., Sotin, C., Thomas, P.C., 2006. Ceres,Vesta, and Pallas: Protoplanets, not asteroids. EOS, Trans. Am. Geophys. Union 87, 105–109. http://dx.doi.org/10.1029/2006EO100002.

McCord, T.B., Castillo-Rogez, J., Rivkin, A., 2011. Ceres: Its origin, evolution and structure and Dawn's potential contribution. Space Sci. Rev. 163, 63–76. http://dx.doi.org/10.1007/s11214-010-9729-9.

McKinnon, W.B., 2008. Could Ceres be a refugee from the Kuiper belt? In: Asteroids, Comets, Meteors Conf., #8389.

McKinnon, W.B., 2012. Where did Ceres accrete? In: Asteroids, Comets, Meteors Conf. #6475.

Melosh, H.J., 1989. Impact Cratering: A Geologic Process. Oxford University Press, New York.

Melosh, H.J., Raefsky, A., 1980. The dynamical origin of subduction zone topography. Geophys. J. R. Astron. Soc. 60, 333–354.

Milliken, R.E., Rivkin, A.S., 2009. Brucite and carbonate assemblages from altered olivine-rich materials on Ceres. Nat. Geol. 2, 258–261. http://dx.doi.org/10.1038/ngeo478.

Millis, R.L., Wasserman, L.H., Franz, O.G., Nye, R.A., Oliver, R.C., Kreidl, T.J., Jones, S.E., Hubbard, W., Lebofsky, L., Goff, R., Marcialis, R., Sykes, M., Frecker, J., Hunten, D., Zellner, B., Reitsema, H., Schneider, G., Dunham, E., Klavetter, J., Meech, K., Oswalt, T., Rafert, J., Strother, E., Smith, J., Povenmire, H., Jones, B., Kornbluh, D., Reed, L., Izor, K., A'Hearn, M.F., Schnurr, R., Osborn, W., Parker, D., Douglas, W.T., Beish, J.D., Klemola, A.R., Rios, M., Sanchez, A., Piironen, J., Mooney, M., Ireland, R.S., Leibow, D., 1987. The size, shape, density, and albedo of Ceres from its occultation of BD+8 deg 471. Icarus 72, 507–518. http://dx.doi.org/10.1016/0019-1035(87)90048-0.

Mohit, P.S., Greenhagen, B.T., McKinnon, W.B., 2012. Polar wander on Ganymede: A possible solution to the apex–antapex cratering conundrum. Wkshp. Early Solar System Impact Bombardment II, # 1649. pp. 51–52.

Ojakangas, G.W., Stevenson, D.J., 1989. Thermal state of an ice shell on Europa. Icarus 81 (October), 220–241. http://dx.doi.org/10.1016/0019-1035(89)90052-3.

Parmentier, E.M., Head, J.W., 1981. Viscous relaxation of impact craters on icy planetary surfaces – Determination of viscosity variation with depth. Icarus 47, 100–111. http://dx.doi.org/10.1016/0019-1035(81)90095-6.

Pathare, A.V., Paige, D.A., Turtle, E., 2005. Viscous relaxation of craters within the martian south polar layered deposits. Icarus 174, 396–418. http://dx.doi.org/10.1016/j.icarus.2004.10.031.

Petrenko, V.F., Whitworth, R.W., 1999. Physics of Ice. Oxford University Press, Oxford.

Pike, R.J., 1980. Control of crater morphology by gravity and target type – Mars, Earth, Moon. Proc. Lunar Sci. Conf. 11, 2159–2189.

Rivkin, A.S., Volquardsen, E.L., 2010. Rotationally-resolved spectra of Ceres in the 3-μm region. Icarus 206, 327–333. http://dx.doi.org/10.1016/j.icarus.2009.08.026.

Rivkin, A.S., Volquardsen, E.L., Clark, B.E., 2006. The surface composition of Ceres: Discovery of carbonates and iron-rich clays. Icarus 185, 563–567. http://dx.doi.org/10.1016/j.icarus.2006.08.022.

Rivkin, A.S. et al., 2011. The surface composition of Ceres. Space Sci. Rev. 163, 95–116. http://dx.doi.org/10.1007/s11214-010-9677-4.

Roscoe, R., 1952. The viscosity of suspensions of rigid spheres. Br. J. Appl. Phys. 3, 267–269.

Rousselot, P. et al., 2011. A search for water vaporization on Ceres. Astron. J. 142, 1–6. http://dx.doi.org/10.1088/0004-6256/142/4/125.

Russell, C.T., Raymond, C.A., 2011. The Dawn mission to Vesta and Ceres. Space Sci. Rev. 163, 3–23. http://dx.doi.org/10.1007/s11214-011-9836-2.

Saint-Pe, O., Combes, M., Rigaut, F., 1993. Ceres surface properties by high-resolution imaging from Earth. Icarus 105, 271–281. http://dx.doi.org/10.1006/icar.1993.1125.

Schenk, P.M., 1991. Ganymede and Callisto – Complex crater formation and planetary crusts. J. Geophys. Res. 96, 15635–15664. http://dx.doi.org/10.1029/91JE00932.

Schenk, P.M., Chapman, C.R., Zahnle, K., Moore, J.M., 2004. Ages and interiors: The cratering record of the Galilean satellites. In: Bagnell, F., Dowling, T., McKinnon, W.B. (Eds.), Jupiter: The Planet, Satellites and Magnetosphere. Cambridge University Press, pp. 427–456.

Schenk, P.M. et al., 2013. Impact crater morphologies on Vesta in Solar System context. Lunar Planet. Sci. 44, p. #2039.

Schorghofer, N., 2008. The lifetime of ice on main belt asteroids. Astrophys. J. 682, 697–705. http://dx.doi.org/10.1086/588633.

Souchez, R.A., Lorrain, R.D., 1991. Ice Composition and Glacier Dynamics. Springer-Verlag, Berlin.

Tedesco, E.F., 1989. Asteroid magnitudes, UBV colors, and IRAS albedos and diameters. In: Binzel, R.P., Gehrels, T., Matthews, M.S. (Eds.), Asteroids II. Univ. Arizona Press, Tucson, AZ, pp. 1090–1138.

Thomas, P.C. et al., 2005. Differentiation of the asteroid Ceres as revealed by its shape. Nature 437, 224–226. http://dx.doi.org/10.1038/nature03938.

Vernazza, P. et al., 2005. Analysis of near-IR spectra of 1 Ceres and 4 Vesta, targets of the Dawn mission. Astron. Astrophys. 436, 1113–1121. http://dx.doi.org/10.1051/0004-6361:20042506.

White, O.L., Schenk, P.M., 2011. Crater shapes on the saturnian satellites: New measurements using Cassini stereo images. Lunar Planet. Sci. 42, #2283.

Zolotov, M.Y., 2009. On the composition and differentiation of Ceres. Icarus 204, 183–193. http://dx.doi.org/10.1016/j.icarus.2009.06.011.